Transit Met Chem (2016) 41:637–645
DOI 10.1007/s11243-016-0063-2

Silver-based coordination complexes of carboxylate ligands: crystal structures, luminescence and photocatalytic properties

Jia Zhang[1] · Chong-Chen Wang[1,2] · Peng Wang[1] · Xin-Xing Guo[1] · Shi-Jie Gao[1]

Received: 21 March 2016 / Accepted: 16 May 2016 / Published online: 2 June 2016

Abstract The complexes $[Ag_4(dpe)_4]\cdot(btec)$ (**1**) and $[Ag_4(bpy)_4]\cdot(btec)\cdot 12H_2O$ (**2**) (dpe = 1,2-di(4-pyridyl)ethylene, bpy = 4,4′-bipyridine, H_4btec = 1,2,4,5-benzenetetracarboxylic acid) have been synthesized in aqueous alcohol/ammonia by slow evaporation at room temperature and characterized by elemental analysis, single-crystal X-ray diffraction, FTIR, UV–Vis and luminescence spectroscopies. Both complexes are composed of 1D infinite cationic $[Ag/dpe(bpy)]_n^{n+}$ chains and discrete $btec^{4-}$ anions. Their three-dimensional supramolecular structures are built up of cationic sheets formed from $[Ag/dpe(bpy)]_n^{n+}$ units via weak Ag…Ag and Ag…N interactions, plus anionic $btec^{4-}$ sheets featuring electrostatic, π–π and hydrogen bonding interactions. Both complexes exhibited photocatalytic activity for the decomposition of methyl orange under UV light irradiation.

Introduction

Over the past decades, coordination complexes built from metal ions as templates and organic ligands as linkers have received much attention, due to their interesting structural features [1–4] and potential applications, such as gas adsorption and separation [5, 6], catalysis [7, 8], drug delivery [9], and so on [10]. In the field of environmental remediation, coordination complexes (including metal–organic frameworks) have been used as efficient adsorbents to remove organic pollutants from wastewater [11], or as photocatalysts for the degradation of organic pollutants [12] or CO_2 as well as reduction of Cr(VI) [13, 14] under UV or visible light irradiation. The self-assembly of such coordination complexes is frequently influenced by several factors including the choice of the organic ligands, metal atoms, counter-ions, reaction temperature, pH and the solvent [15–17]. In particular, the shape, functionality and flexibility of the ligands can play a crucial role in the rational design of structures with specific physical and/or chemical properties [18]. As excellent bidentate N-donor bridging ligands, 1,2-di(4-pyridyl)ethylene (dpe) and 4,4′-bipyridine (bpy) have been used to construct various frameworks [19, 20]. Also, carboxylate ligands (such as H_4btec, as depicted in Scheme 1) are often used as multifunctional organic linkers due to their flexible coordination modes and ability to act as hydrogen bond acceptors and donors [21–24].

In addition to the above considerations, the size, coordination ability, and supramolecular interactions of counter-ions, especially anions, can exert various influences on the structures of the resulting coordination complexes. Considering that organic carboxylate anions are more numerous and versatile than inorganic anions [25], our group has focused its efforts on the construction of silver coordination compounds composed of various carboxylate anions, in order to investigate how the self-assembly process can be effected by different organic anions [26–28].

In this paper, two coordination complexes, namely $[Ag_4(dpe)_4]\cdot(btec)$ (**1**), and $[Ag_4(bpy)_4]\cdot(btec)\cdot 12H_2O$ (**2**), have been constructed from dpe/bpy and 1,2,4,5-benzenetetracarboxylic acid (H_4btec) ligands. The

✉ Chong-Chen Wang
chongchenwang@126.com

[1] Key Laboratory of Urban Stormwater System and Water Environment (Ministry of Education), Beijing University of Civil Engineering and Architecture, Beijing 100044, China

[2] Beijing Engineering Research Center of Sustainable Urban Sewage System Construction and Risk Control, Beijing University of Civil Engineering and Architecture, Beijing 100044, China

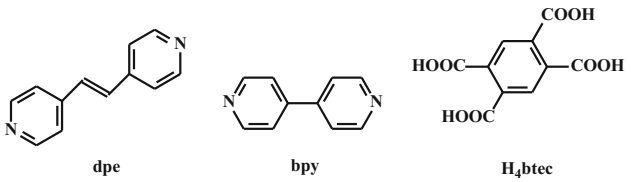

Scheme 1 The structural formulae of dpe, bpy and H_4btec

supramolecular structures of these complexes are presented and discussed. In addition, their optical, luminescent and photocatalytic properties have been investigated.

Experimental

Materials and methods

All chemicals of reagent grade were commercially available and used without further purification. CHO elemental analyses were obtained with an Elementar Vario EL-III instrument. FTIR spectra were recorded from 400 to 4000 cm^{-1} on a Nicolet 6700 FTIR spectrophotometer as KBr pellets. UV–Vis diffuse reflectance spectra (UV–Vis DRS) of solid samples were measured between 200 and 800 nm with a Perkin Elmer Lamda 650S spectrophotometer using $BaSO_4$ as the standard with 100 % reflectance. Powder X-ray diffraction (PXRD) patterns were recorded using a Dandonghaoyuan DX-2700B diffractometer employing Cu Kα radiation. Luminescence spectra were obtained on a Hitachi F-7000 fluorescence spectrophotometer equipped with a xenon flash lamp at room temperature.

Synthesis of complex 1

An ammonia solution (125 mL, 0.5 mol/L) of $AgNO_3$ (0.21 g, 1.25 mmol) and H_4btec (0.32 g, 1.25 mmol) was added dropwise to an EtOH solution (125 mL) of dpe (0.23 g, 1.25 mmol), and the mixture was stirred for 15 min, then allowed to evaporate slowly at room temperature in the dark. Block-like white crystals of $[Ag_4(dpe)_4]\cdot(btec)$ (**1**) were obtained after 4 weeks (yield 93 % based on $AgNO_3$). Anal. Calcd. for $C_{58}H_{42}Ag_4N_8O_8$(%): C, 49.4; H, 3.0; N, 7.9. Found: C, 49.2; H, 3.2; N, 7.9. IR (KBr)/cm^{-1}: 3431(s), 1600(s), 1498(m), 1416(m), 1376(m), 1326(w), 1283(w), 1205(w), 1134(w), 1074(w), 1010(m), 998(w), 973(m), 955(w), 862(w), 827(m), 772(w), 669(w), 548(w).

Synthesis of complex 2

Synthesis of block-like white crystals of $[Ag_4(bpy)_4]\cdot(btec)\cdot 12H_2O$ (**2**) followed the same procedure as for **1**, except that dpe was replaced with bpy (yield 87 % based on $AgNO_3$). Anal. Calcd. for $C_{50}H_{58}Ag_4N_8O_{20}$ (%): C, 39.4; H, 3.8; N, 7.4. Found: C, 39.3; H, 4.0; N, 7.3. IR (KBr)/cm^{-1}: 3387(s), 3052(m), 3028(m), 1954(w), 1599(s), 1527(m), 1488(m), 1411(s), 1373(s), 1326(m), 1314(m), 1282(w), 1223(m), 1134(w), 1091(w), 1071(w), 1040(w), 1001(w), 992(w), 962(w), 940(w), 861(w), 846(w), 828(w), 804(s), 772(w), 732(w), 667(w), 621(m), 577(w), 564(m), 509(m).

X-ray crystallography

X-ray single-crystal data for both complexes were recorded with a Bruker Smart 1000 CCD area detector diffractometer with graphite-monochromatized Mo$K\alpha$ radiation ($\lambda = 0.71073$ Å) using φ–ω mode at 298(2) K. The SMART program [29] was used for data collection and SAINT software [30] was used to extract data. Empirical absorption corrections were performed with the SADABS program [31]. The structures were solved by direct methods (SHELXS-97) [32] and refined by full-matrix-least squares techniques on F^2 with anisotropic thermal parameters for all of the non-hydrogen atoms (SHELXL-97) [32]. All hydrogen atoms were located by Fourier difference synthesis and geometrical analysis and were allowed to ride on their respective parent atoms. All structural calculations were carried out using the SHELX-97 program package [32]. Crystallographic data and structural refinements for both complexes are summarized in Table 1. Selected bond lengths and angles are listed in Table 2.

Photocatalysis experiments

Methyl orange (MO), a typical organic dye, was selected as a model pollutant to evaluate the photocatalytic performance of the complexes under UV light irradiation in a photocatalytic reaction system (Beijing Aulight Co. Ltd). A solid sample (50 mg) of the required complex was added to 200 mL of aqueous MO solution (10 mg/L) in a 300-mL breaker. The suspension was magnetically stirred in the dark for 120 min to ensure the establishment of an adsorption/desorption equilibrium before the onset of photocatalysis. During the photocatalytic degradation experiment, 1 mL aliquots were extracted using a 0.45 μm syringe filter (Shanghai Troody) at regular intervals for analysis. A Laspec Alpha-1860 spectrometer was used to monitor the MO concentration changes determined by the maximum absorbance at 463 nm.

Results and discussion

Both complexes **1** and **2** were stable and insoluble in water and common organic solvents, including but not limited to methanol, ethanol, ether and *N,N*-dimethylformamide

Table 1 Details of X-ray data collection and refinement for compounds **1** and **2**

	1	**2**
Formula	$C_{58}H_{42}Ag_4N_8O_8$	$C_{50}H_{58}Ag_4N_8O_{20}$
M	1410.48	1522.52
Crystal system	Triclinic	Triclinic
Space group	Pī	Pī
a (Å)	10.8200(9)	9.6340(9)
b (Å)	12.4419(11)	12.8210(11)
c (Å)	14.1031(12)	13.4077(12)
α (°)	65.6890(10)	115.833(2)
β (°)	78.061(2)	91.2510(10)
γ (°)	71.8090(10)	107.868(3)
V (Å^3)	1637.0(2)	1395.1(2)
Z	1	1
μ (Mo, Kα) (mm^{-1})	1.231	1.466
Total reflections	5647	7158
Unique	5647	4848
F(000)	698	762
Goodness-of-fit on F^2	1.085	1.092
R_{int}	0.0000	0.0320
R_0	0.1388	0.0601
ωR_2	0.3402	0.1510
R_1 (all data)	0.1990	0.1088
ωR_2 (all data)	0.3708	0.1655
Largest diff. peak and hole (e/Å^3)	2.390, −2.179	1086, −0.853

Table 2 Selected bond lengths (Å) and angles (°) for compound **1** and **2**

1[a]		**2**[b]	
Bond lengths (Å)			
Ag(1)–N(1)	2.138(13)	Ag(1)–N(1)	2.146(6)
Ag(1)–N(2)#1	2.153(11)	Ag(1)–N(3)	2.147(6)
Ag(2)–N(3)	2.123(12)	Ag(2)–N(2)	2.136(6)
Ag(2)–N(4)#1	2.149(11)	Ag(2)–N(4)	2.144(6)
N(2)–Ag(1)#2	2.153(11)		
N(4)–Ag(2)#2	2.149(11)		
Bond angles (°)			
N(1)–Ag(1)–N(2)#1	174.8(4)	N(1)–Ag(1)–N(3)	178.6(2)
N(3)–Ag(2)–N(4)#1	175.8(5)	N(2)–Ag(2)–N(4)	174.6(2)

[a] Symmetry transformations used to generate equivalent atoms: #1 $x-1, y+1, z$; #2 $x+1, y-1, z$; #3 $-x+1, -y+1, -z+1$

[b] Symmetry transformations used to generate equivalent atoms: #1 $-x+1, -y+1, -z+1$; #2 $x+1, y+1, z-1$; #3 $x-1, y-1, z+1$

(DMF). In the FTIR spectra of both complexes, a strong and broad absorption at 3387 cm^{-1} is assigned to the O–H stretching vibration of lattice water molecules. The absence of an absorption peak around 1500 cm^{-1} from H_4btec indicates that the carboxyl groups are completely deprotonated. The positions of the stretching COO vibrations at 1600 ($\nu_{as(COO)}$) and 1416 ($\nu_{s(COO)}$) for **1** and 1599 ($\nu_{as(COO)}$) and 1411 ($\nu_{s(COO)}$) cm^{-1} for **2**, for which the corresponding $\Delta\nu$ values are both ca. 200 cm^{-1}, suggests that the COO^- groups are terminal and not coordinated to the Ag^+ centers [33].

Crystallographic analysis of complex 1

The crystal structure analysis reveals that $[Ag_4(dpe)_4]$-(btec) (**1**) is made up of 1-D cationic $[Ag_4(dpe)_4]_n^{4n+}$ chains and discrete btec^{4-} counter-ions. As illustrated in Fig. 1a, atoms Ag1 and Ag2 are linearly coordinated by two N atoms from two different dpe ligands, with N–Ag–N angles of 174.8(4)° and 175.8(5)°, and Ag–N distances ranging from 2.123(12) to 2.153(11) Å, which are comparable with the Ag–N bond distances reported in similar coordination compounds [34, 35]. Similar to the known complexes $[Ag_2(dpe)_2(H_2O)_2](dpadc)\cdot H_2O$ and $[Ag_6(dpe)_6(H_2O)_4]\cdot(tp)_3\cdot 12H_2O$ [28], the dpe acts as a typical *N,N′*-bidentate ligand to join Ag(I) atoms into 1D cationic chains. The two pyridyl rings are nearly coplanar, such that the corresponding dihedral angles are 5.0° and 5.2°. In distinct contrast to its role as a ligand in the complexes $\{[Co_{1.5}(Hbtec)(L1)_{1.5}(H_2O)_2]\cdot(H_2O)\}_n$ and $\{[Co(H_2btec)(L2)]\cdot(L2)_{0.5}(H_2O)_2\}_n$ [24], the completely deprotonated btec^{4-} in complex **1** only acts as a counter-ion to compensate the

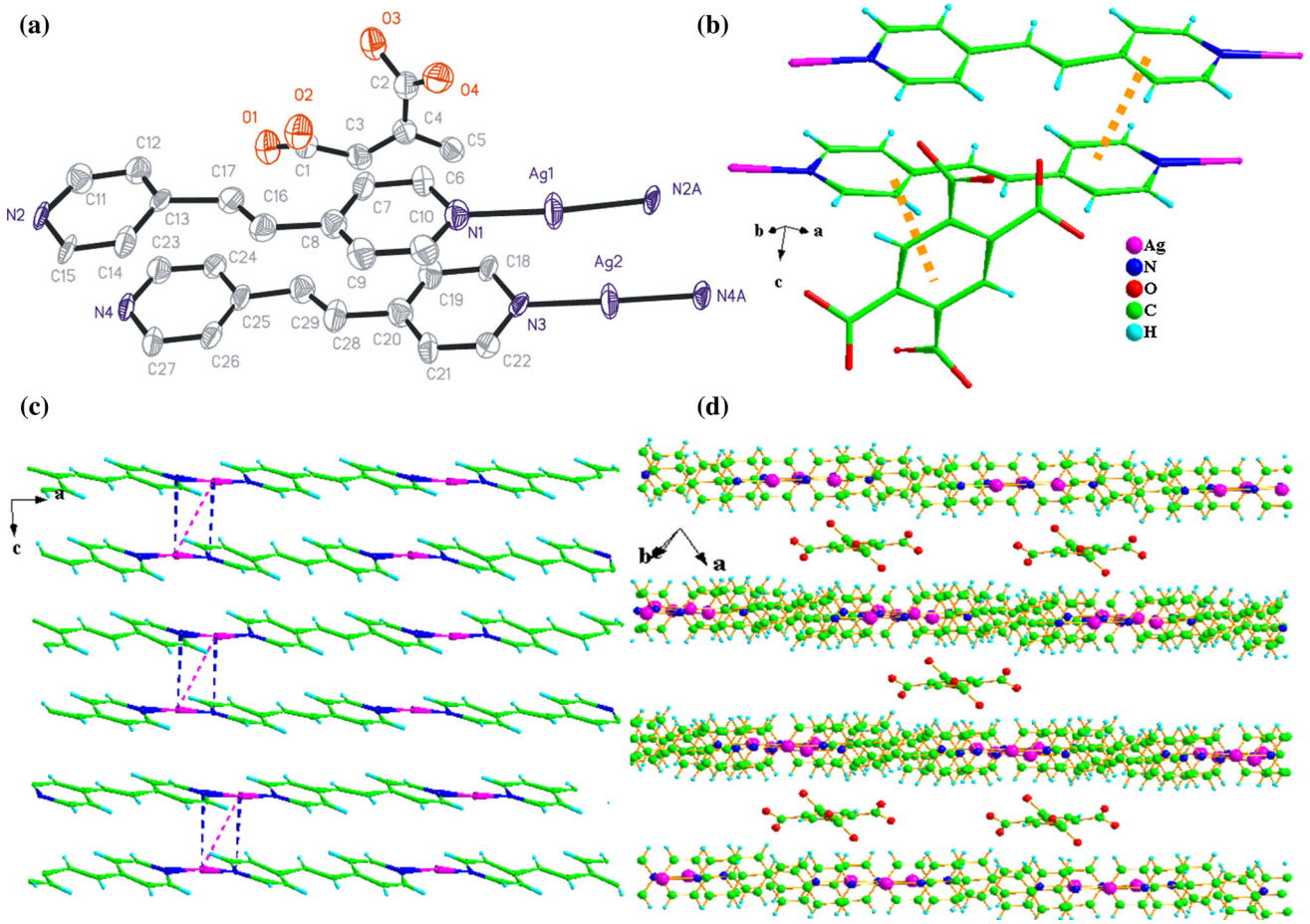

Fig. 1 **a** Asymmetric unit of $[Ag_4(dpe)_4]\cdot(btec)$ (**1**) and coordination environments around the Ag^I atoms. H atoms are omitted for clarity. **b** Packing view of the framework assembled with the aid of π–π stacking interaction for complex **1**. **c** The cationic layer formed from Ag-dpe chains in complex **1**. **d** Packing view of the sandwich-like framework along the *c*-axis for compound **1**.

cationic charge of the 1D $[Ag_4(dpe)_4]_n^{4n+}$ chains, without participating in the construction of a higher dimensional structure.

The adjacent cationic chains are joined into 2D cationic sheets $[Ag(dpe)]_n^{n+}$ via weak Ag…Ag interactions [Ag…Ag distance is 3.4252(20) Å), also Ag…N contacts with distances of 3.4244(103) and 3.3745(105) Å] and π–π stacking interactions (Cg(1)…Cg(3) = 3.660(10) Å, where Cg(1) is the centroid of N(2)/C(11)/C(12)/C(13)/C(14)/C(15), and Cg(3) is the centroid of N(4)/C(23)/C(24)/C(25)/C(26)/C(27)), as depicted in Fig. 1c and Table 4. Finally, a 3D supramolecular sandwich-like structure is constructed with the aid of electrostatic and π–π stacking interactions, with centroid–centroid distances of 3.632(9) Å [where Cg(2) is the centroid of N(3)/C(18)/C(19)/C(20)/C(21)/C(22) and Cg(4) is the centroid of C(3)/C(4)/C(5)/C(3)a/C(4)a/C(5)a] between 1D cationic chains $[Ag_2(dpe)]_\infty^{n+}$ and the fully deprotonated $btec^{4-}$ anions (Fig. 1b, d; Table 4).

Crystallographic analysis of complex 2

Complex **2** is made up of cationic chains of $[Ag_4(bpy)_4]_n^{4n+}$, completely deprotonated $btec^{4-}$ anions and twelve lattice water molecules. In the $[Ag_4(bpy)_4]_n^{4n+}$ chains, each Ag(I) atom is interconnected with two nitrogen atoms from two different rigid bpy ligands in a linear coordination geometry [Ag–N bond lengths ranging from 2.136(6) to 2.147(6) Å and N–Ag–N angles of 178.6(2) and 174.6(2)°], as illustrated in Fig. 2a and Table 2. The cationic charge of the $[Ag_4(bpy)_4]_n^{4n+}$ chains is balanced by the completely deprotonated $btec^{4-}$ anions.

In complex **2**, the adjacent $[Ag_4(bpy)_4]_n^{4n+}$ chains are packed into cationic sheets (A) via ligand-unsupported Ag…Ag = 3.5878(8) Å and Ag…N = 3.8550(52) Å contacts, as illustrated in Fig. 2b. This arrangement is similar to previously reported Ag^I complexes [28]. The anionic sheets (B) are constructed from $btec^{4-}$ and water molecules via abundant intermolecular hydrogen bonding

interactions (Fig. 2c; Table 3). The cationic A sheets and anionic B sheets are further linked by π–π stacking and electrostatic interactions to build up a 3D sandwich-like crystal framework in the order of "…ABAB…", as illustrated in Fig. 2d, similar to previously reported compounds [27, 36].

Optical energy gap

To investigate the conductivities of these complexes and to obtain band gap E_g values, their UV–visible diffuse reflectance spectra were measured [37]. The E_g values were determined as the intersection point between the energy axis and the line extrapolated from the linear portion of the absorption edge in a plot of the Kubelka–Munk function as listed in Eq. (1):

$$F = (1 - R)^2/2R \quad (1)$$

where R is the reflectance of an infinitely thick layer at a given wavelength [38]. The plots of F versus E for complexes **1** and **2** are illustrated in Fig. 3a, where steep absorption edges are displayed, and the E_g values were calculated at 3.2 and 3.4 eV for **1** and **2**, respectively, implying selective absorption in the ultraviolet region for both complexes [39]. This is confirmed by their absorption spectra, as shown in Fig. 3b.

Fluorescence properties

The solid-state luminescent emission properties of complexes **1** and **2** were investigated (Fig. 4a), giving maximum emission bands at 403 nm (λ_{ex} = 300 nm) for **1**, plus

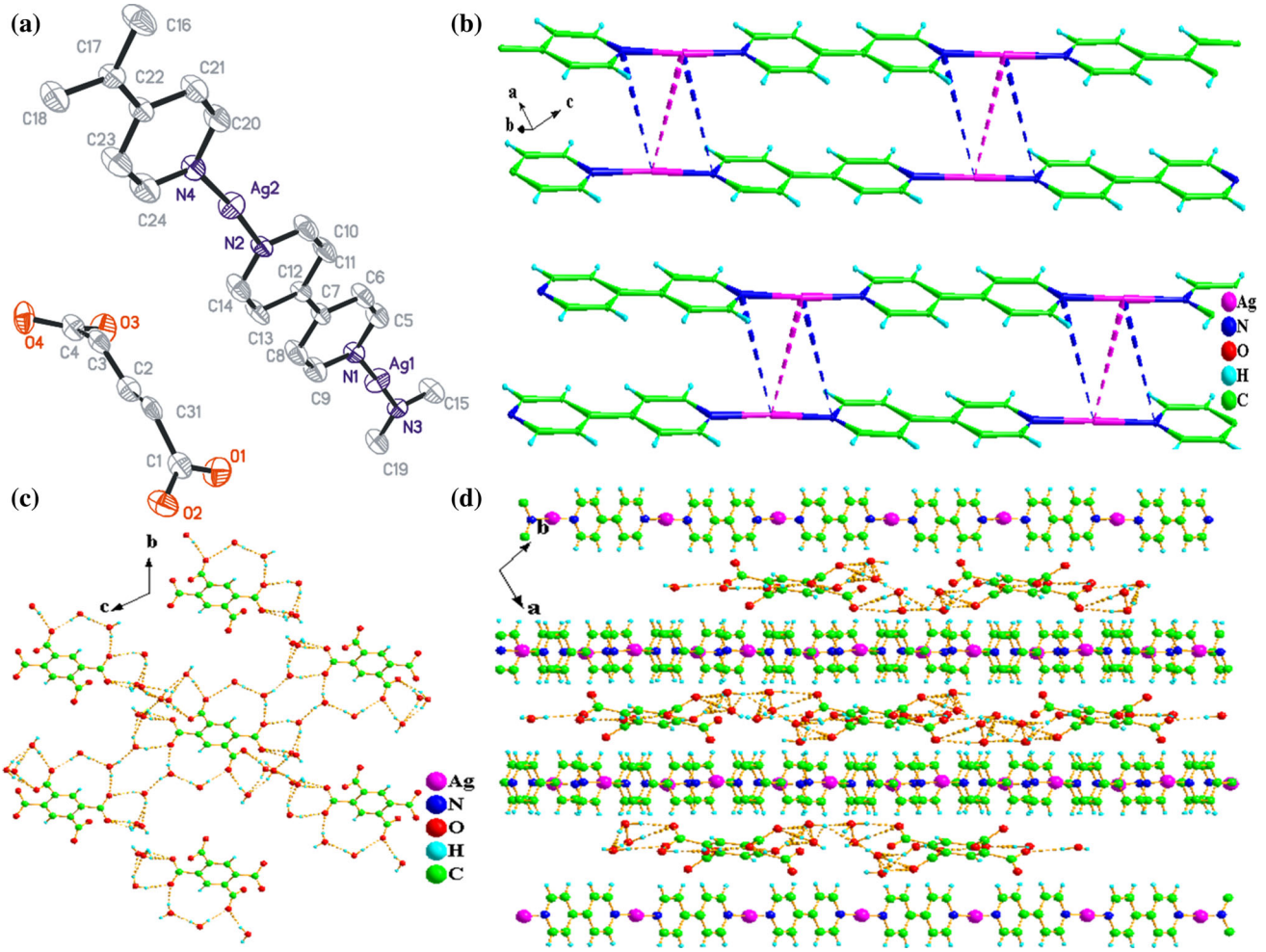

Fig. 2 **a** Asymmetric unit of $[Ag_4(bpy)_4]\cdot(btec)\cdot 12H_2O$ (**2**) and coordination environments around the Ag^I atoms. Water molecules and corresponding H atoms are omitted for clarity. **b** The cationic layer formed from Ag-bpy chains in complex **2**. **c** The anionic layer constructed from $btec^{4-}$ and water molecules in complex **2**. **d** Packing view of the sandwich-like framework built from anionic and cationic sheets along the *c*-axis for compound **2**

Table 3 Hydrogen bonds for compound **2** [Å and °]

D–H	*d*(D–H)	*d*(H…A)	<DHA	*d*(D…A)	A
O5–H5C	0.850	1.860	162.79	2.684	O3
O5–H5D	0.850	1.919	162.23	2.741	O7 [$-x+1, -y+1, -z$]
O6–H6C	0.850	1.855	174.90	2.703	O1
O6–H6D	0.850	1.893	173.97	2.739	O5
O7–H7C	0.850	2.015	159.67	2.828	O3
O7–H7D	0.850	2.083	139.15	2.782	O9′_b
O7–H7D	0.850	2.116	159.60	2.928	O9_a
O8–H8C	0.850	2.035	166.47	2.869	O1
O8–H8D	0.850	1.920	168.14	2.758	O6 [$-x+2, -y+2, -z+1$]
O9–H9C_a	0.850	1.844	144.91	2.586	O10_a [$x, y-1, z-1$]
O9–H9D_a	0.850	1.974	145.58	2.718	O4
O10–H10E_a	0.850	1.867	165.57	2.698	O2 [$x-1, y, z$]
O10–H10F_a	0.850	2.063	167.13	2.898	O8 [$x-1, y, z$]
O9′–H9′C_b	0.850	1.969	164.77	2.798	O4
O9′–H9′D_b	0.850	1.641	164.22	2.470	O10′_b [$-x, -y+1, -z+1$]
O10′–H10G_b	0.850	2.081	163.32	2.905	O2 [$x-1, y, z$]
O10′–H10H_b	0.850	2.077	164.38	2.905	O8 [$x-1, y, z$]

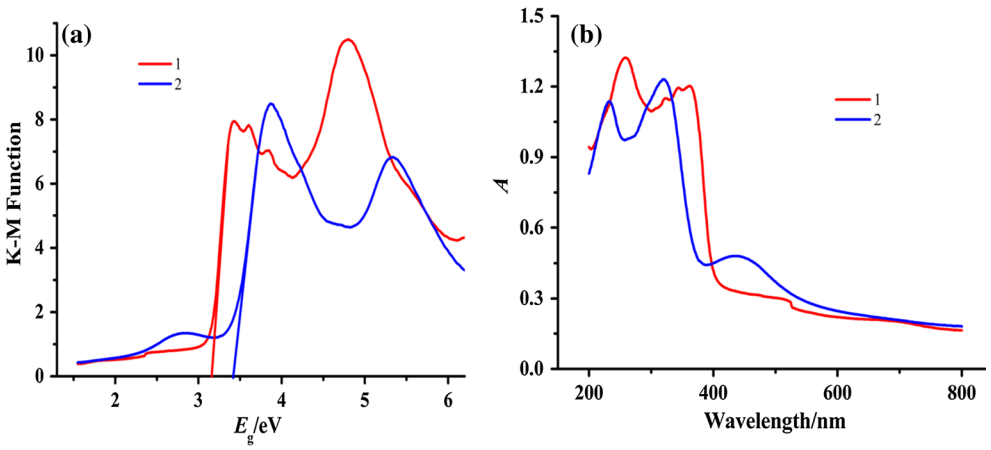

Fig. 3 **a** UV–visible diffuse reflectance spectra of complexes **1** and **2**. **b** Kubelka–Munk-transformed diffuse reflectance spectra of complexes **1** and **2**

355 and 372 nm ($\lambda_{ex} = 325$ nm) for **2**. According to the literature [22, 40], these luminescence properties can be attributed to Ag…Ag interactions and ligand-to-metal charge transfer.

For the purpose of checking the phase purities of the samples which were used to study the fluorescence properties, powder X-ray diffraction (PXRD) patterns have been checked at ambient temperature, as shown in Fig. 4b, c. For both complexes, the measured PXRD patterns agreed well with those calculated from the X-ray single-crystal diffraction data, confirming their phase purities. The slight differences in intensities can be attributed to the preferred orientations of the crystalline powder samples [41].

Photocatalytic activities

The photocatalytic performance of these complexes for the degradation of MO under UV irradiation was assessed. In addition, control experiments for MO degradation in the absence of catalyst were performed and the efficiencies of

Table 4 Defined ring and relative parameters of the π–π interactions in compounds **1** and **2**

Compound **1**				
Cg(1): N(2) → C(11) → C(12) → C(13) → C(14) → C(15)→ Cg(2): N(3) → C(18) → C(19) → C(20) → C(21) → C(22)→ Cg(3): N(4) → C(23) → C(24) → C(25) → C(26) → C(27)→ Cg(4): C(3) → C(4) → C(5) → C(3)a → C(4)a → C(5)a→				
Cg(I) Cg(J)	Dist. centroids (Å)	Dihedral angle (°)	Perp. dist. (IJ) (Å)	Perp. dist. (JI) (Å)
Cg(1) → Cg(3)^{i*}	3.660(10)	7.1(8)	−3.476(7)	3.377(7)
Cg(2) → Cg(4)^{i*}	3.632(9)	5.1(8)	−3.550(6)	3.460(6)
Symmetry codes: (i) x, y, z				
Compound **2**				
Cg(1): N(2) → C(10) → C(11) → C(12) → C(13) → C(14)→ Cg(2): N(3) → C(15) → C(16)c → C(17)c → C(18)c → C(19)→ Cg(3): N(4) → C(20) → C(21) → C(22) → C(23) → C(24)→ Cg(4): C(16) → C(17) → C(18) → C(19)b → N(3)b → C(15)b→ Cg(5): C(2) → C(3) → C(31)a → C(2)a → C(3)a → C(31)→				
Cg(I) Cg(J)	Dist. centroids (Å)	Dihedral angle (°)	Perp. dist. (IJ) (Å)	Perp. dist. (JI) (Å)
Cg(1) → Cg(2)^{i*}	3.635(5)	1.2(4)	3.565(4)	3.572(4)
Cg(1) → Cg(3)^{ii*}	3.664(5)	2.0(4)	−3.600(4)	−3.600(4)
Cg(1) → Cg(5)^{iii*}	3.664(5)	2.0(4)	−3.600(4)	−3.600(4)
Cg(2) → Cg(4)^{iii*}	3.631(5)	1.8(4)	−3.568(4)	−3.574(4)
Cg(3) → Cg(4)^{i*}	3.663(5)	0.9(4)	3.601(4)	3.604(4)
Cg(4) → Cg(5)^{iiii*}	3.663(5)	0.9(4)	3.604(4)	3.602(4)
Symmetry codes: (i) $1-x$, $2-y$, $1-z$; (ii) $1-x$, $2-y$, $-z$; (iii) $-x$, $1-y$, $1-z$; (iiii) $-x$, $1-y$, $2-z$				

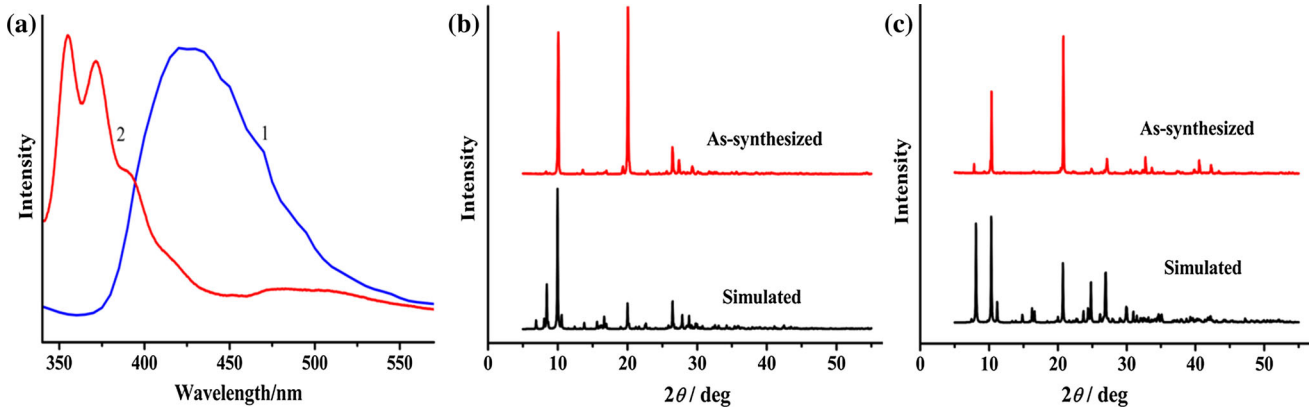

Fig. 4 **a** Luminescent emission spectra of complexes **1** and **2** in the solid state at room temperature. **b** PXRD pattern of complex **1** versus the simulated XRD pattern from the single-crystal structure data. **c** PXRD pattern of complex **2** versus the simulated XRD pattern from the single-crystal structure data

MO degradation by the complexes in the dark and under Hg lamp irradiation were investigated, as shown in Fig. 5.

Both complexes exhibited photocatalytic activity for MO degradation under UV irradiation for 120 min, as shown in Fig. 5a, increasing from 17.8 % (without any catalyst) to 52.3 % for **1** and 26.5 % for **2**. For both complexes, the photocatalytic degradation reactions obeyed a pseudo-first-order kinetic model with $R^2 = 0.9596$ and 0.9892 for **1** and **2**, respectively, giving rate constants (k) of 0.0058 and 0.0021 min^{-1},

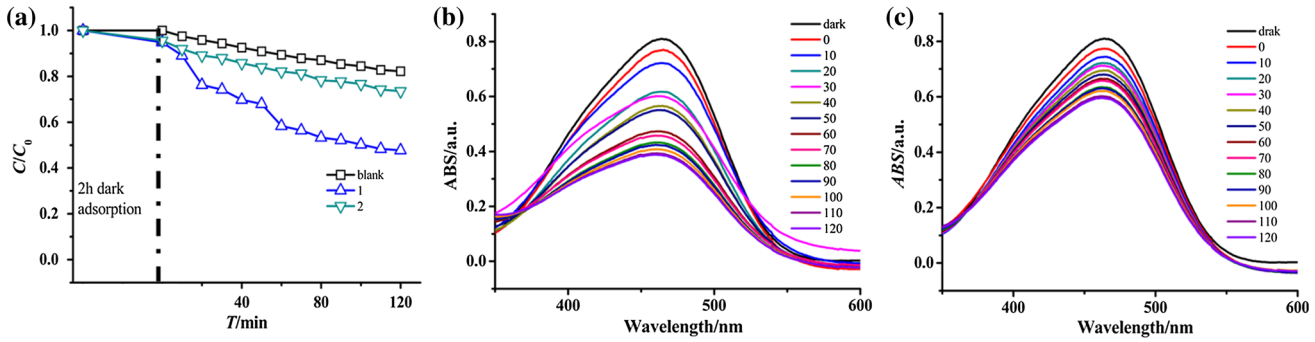

Fig. 5 **a** Plots of MO concentration versus irradiation time in the dark and under irradiation by Hg lamp in the presence of complexes **1** and **2**. **b** UV–Vis absorption spectra of an MO solution during the photocatalytic reaction under Hg lamp irradiation in the presence of complex **1**. **c** UV–Vis absorption spectra of an MO solution during the photocatalytic reaction under Hg lamplight irradiation in the presence of complex **2**

respectively, as evidenced by linear plots of $\ln(C/C_0)$ versus reaction time t.

Conclusions

In summary, the silver(I) complexes reported in this paper both contain sandwich-like frameworks, in which the bidentate dpe and bpy ligands join the Ag(I) centers into 1D cationic $[Ag(L)]_n^{n+}$ chains, charge balanced by $btec^{4-}$ anions. The ligand-unsupported Ag…Ag and Ag…N interactions, plus hydrogen bonding and/or π–π stacking interactions, mediate the construction of 3D sandwich-like structures. Both complexes possess nearly identical optical energy gaps and good luminescence properties, but show different photocatalytic properties for the decomposition of MO. Our laboratory is currently engaged in further research to explore the photocatalytic properties of these complexes for the decomposition of other organic pollutants.

Supplementary materials

CCDC 1447561 and 1447560 contain the supplementary crystallographic data for complexes **1** and **2**, respectively. These data can be obtained free of charge from the Cambridge Crystallographic Data Centre via www.ccdc.cam.ac.uk/data_request/cif, or from the Cambridge Crystallographic Data Centre, 12 Union Road, Cambridge CB2 1EZ, UK; fax: (+44) 1223-336-033; or e-mail: deposit@ccdc.cam.ac.uk.

Acknowledgments We thank the financial support from National Natural Science Foundation of China (51578034), the Beijing Natural Science Foundation & Scientific Research Key Program of Beijing Municipal Commission of Education (KZ201410016018, KM201510016017), the Training Program Foundation for the Beijing Municipal Excellent Talents(2013D005017000004), and the Importation & Development of High-Caliber Talents Project of Beijing Municipal Institutions (CIT&CD201404076), 2011 Project for Cooperation & Innovation under the Jurisdiction of Beijing Municipality.

References

1. Wang C-C, Zhang Y-Q, Zhu T, Zhang X-Y, Wang P, Gao S-J (2015) Four coordination compounds constructed from 1,10-phenanthroline and semi-flexible and flexible carboxylic acids: hydrothermal synthesis, optical properties and photocatalytic performance. Polyhedron 90:58–68
2. Wang C-C, Jing H-P, Wang P, Gao S-J (2015) Series metal–organic frameworks constructed from 1,10-phenanthroline and 3,3′,4,4′-biphenyltetracarboxylic acid: hydrothermal synthesis, luminescence and photocatalytic properties. J Mol Struct 1080:44–51
3. Hao J-M, Zhao Y-N, Li H-H, Ming C-L, Cui G-H (2015) Synthesis, structures, and characterization of two d^{10} metal coordination polymers with a flexible bis(triazole) ligand. Synth React Inorg M 45(7):947–951
4. Xiao S-L, Qin L, He C-H, Du X, Cui G-H (2013) Synthesis, characterizations and luminescent properties of two cadmium (II) coordination polymers derived from bis (benzimidazole)-based ligands. J Inorg Organomet Polym Mater 3(3):771–778
5. Rowsell JL, Spencer EC, Eckert J, Howard JA, Yaghi OM (2005) Gas adsorption sites in a large-pore metal–organic framework. Science 309(5739):1350–1354
6. Rosi NL, Eckert J, Eddaoudi M, Vodak DT, Kim J, O'Keeffe M, Yaghi OM (2003) Hydrogen storage in microporous metal–organic frameworks. Science 300(5622):1127–1129
7. Wang C-C, Du X-D, Li J, Guo X-X, Wang P, Zhang J (2016) Photocatalytic Cr(VI) reduction in metal–organic frameworks: a mini-review. Appl Catal B-Environ 193C:198–216
8. Shen L, Huang L, Liang S, Liang R, Qin N, Wu L (2014) Electrostatically derived self-assembly of NH_2-mediated zirconium MOFs with graphene for photocatalytic reduction of Cr (vi). RSC Adv 4(5):2546–2549
9. Horcajada P, Chalati T, Serre C, Gillet B, Sebrie C, Baati T, Eubank JF, Heurtaux D, Clayette P, Kreuz C (2010) Porous metal-organic-framework nanoscale carriers as a potential platform for drug delivery and imaging. Nat Mater 9(2):172–178
10. So MC, Wiederrecht GP, Mondloch JE, Hupp JT, Farha OK (2015) Metal–organic framework materials for light-harvesting and energy transfer. Chem Commun 51(17):3501–3510

11. Zhang Y-Q, Wang C-C, Zhu T, Wang P, Gao S-J (2015) Ultra-high uptake and selective adsorption of organic dyes with a novel polyoxomolybdate-based organic–inorganic hybrid compound. RSC Adv 5(57):45688–45692
12. Wang C-C, Li J-R, Lv X-L, Zhang Y-Q, Guo G (2014) Photocatalytic organic pollutants degradation in metal–organic frameworks. Energy Environ Sci 7(9):2831–2867
13. Shen L, Liang S, Wu W, Liang R, Wu L (2013) Multifunctional NH_2-mediated zirconium metal–organic framework as an efficient visible-light-driven photocatalyst for selective oxidation of alcohols and reduction of aqueous Cr (vi). Dalton Trans 42(37):13649–13657
14. Wang C-C, Zhang Y-Q, Li J, Wang P (2015) Photocatalytic CO_2 reduction in metal–organic frameworks: a mini review. J Mol Struct 1083C:127–136
15. Han L-J, Kong Y-J, Sheng N (2015) Crystal structure, infrared spectra and luminescence of a 1D Cd coordination polymer with 4-nitrophthalic acid and 1,10-phenanthroline monohydrate ligands. Opt Spectrosc 118(1):60–66
16. Wang X-L, Sui F-F, Lin H-Y, Xu C, Liu G-C, Zhang J-W, Tian A-X (2013) Role of aromatic dicarboxylates in the structural diversity of cobalt (ii) and copper (ii) coordination polymers containing a flexible N, N′-di (3-pyridyl) octanediamide ligand. CrystEngComm 15(36):7274–7284
17. Hou S, Liu Q-K, Ma J-P, Dong Y-B (2013) Cd (II)-coordination framework: synthesis, anion-induced structural transformation, anion-responsive luminescence, and anion separation. Inorg Chem 52(6):3225–3235
18. Yang J, Ma J-F, Batten SR (2012) Polyrotaxane metal–organic frameworks (PMOFs). Chem Commun 48(64):7899–7912
19. Ghosh SK, Ribas J, Bharadwaj PK (2005) Characterization of 3-D metal–organic frameworks formed through hydrogen bonding interactions of 2-D networks with rectangular voids by Co^{II}- and Ni^{II}-pyridine-2, 6-dicarboxylate and 4, 4′-bipyridine or 1, 2-di (pyridyl) ethylene. Cryst Growth Des 5(2):623–629
20. Burd SD, Ma S, Perman JA, Sikora BJ, Snurr RQ, Thallapally PK, Tian J, Wojtas L, Zaworotko MJ (2012) Highly selective carbon dioxide uptake by $[Cu(bpy\text{-}n)_2(SiF6)]$(bpy-1 = 4,4′-Bipyridine; bpy-2 = 1, 2-bis(4-pyridyl) ethene). J Am Chem Soc 134(8):3663–3666
21. Wang C-C, Li H-Y, Guo G-L, Wang P (2013) Synthesis, characterization, and luminescent properties of a series of silver (I) complexes with organic carboxylic acid and 1,3-bis(4-pyridyl) propane ligands. Transit Met Chem 38(3):275–282
22. Zhang J, Wang C-C, Wang P, Gao S-J (2015) Three silver complexes constructed from organic carboxylic acid and 1,2-bis (4-pyridyl) ethane ligands: syntheses, crystal structures, and luminescent properties. Transit Met Chem 40(8):821–829
23. Han X-H, Li M-F, Wang D-L, Song X, Jiang B, Sun Y-G (2011) Two novel coordination polymers based on 1,2,3,4-butanetetracarboxylic acid: synthesis, structure, and luminescence properties. Inorg Chem Commun 14(9):1323–1328
24. Hao JM, Li YH, Li HH, Cui GH (2014) Two cobalt (II) metal–organic frameworks based on mixed 1,2,4,5-benzenetetracarboxylic acid and bis (benzimidazole) ligands. Transit Met Chem 39(1):1–8
25. Wang X, Chen Y, Liu G, Lin H, Zhang J (2009) Organic carboxylate anions effect on the structures of a series of Mn(II) complexes based on 2-phenylimidazo [4, 5-f] 1,10-phenanthroline ligand. J Solid State Chem 182(9):2392–2401
26. Wang C-C, Guo G-L, Wang P (2013) Synthesis, structure, and luminescent properties of three silver (I) complexes with organic carboxylic acid and 4,4′-bipyridine-like ligands. Transit Met Chem 38(4):455–462
27. Wang C-C, Wang P, Feng L-L (2012) Influence of organic carboxylic acids on self-assembly of silver (I) complexes containing 1,2-bis(4-pyridyl) ethane ligands. Transit Met Chem 37(2):225–234
28. Wang C-C, Wang P, Guo G-L (2012) 3D sandwich-like frameworks constructed from silver chains: synthesis and crystal structures of six silver (I) coordination complexes. Transit Met Chem 37(4):345–359
29. Bruker AXS (2000) SMART, Version 5.611. Bruker AXS, Madison
30. Bruker AXS (2003) SAINT, Version 6.28. Bruker AXS, Madison
31. SADABS (2000) V2.03. Bruker AXS, Madison
32. Sheldrick GM (1997) SHELX-97. Göttingen University, Germany
33. Deacon G, Phillips R (1980) Relationships between the carbon-oxygen stretching frequencies of carboxylato complexes and the type of carboxylate coordination. Coord Chem Rev 33(3):227–250
34. Nandy M, Banerjee S, Rizzoli C, Zangrando E, Nonat A, Charbonnière LJ, Mitra S (2013) Syntheses, structural diversity and photo-physical properties of copper (I) and silver (I) coordination polymers based on the pyridine-4-amidoxime ligand. Polyhedron 65:252–261
35. Di Nicola C, Marchetti F, Nervi C, Pettinari C, Robinson WT, Sobolev AN, White AH (2010) Syntheses, structures and spectroscopy of uni-and bi-dentate nitrogen base complexes of silver (i) trifluoromethanesulfonate. Dalton Trans 39(3):908–922
36. Wang C-C, Jing H-P, Wang P (2014) Three silver-based complexes constructed from organic carboxylic acid and 4,4′-bipyridine-like ligands: syntheses, structures and photocatalytic properties. J Mol Struct 1074:92–99
37. Du P, Yang Y, Yang J, Liu B-K, Ma J-F (2013) Syntheses, structures, photoluminescence, photocatalysis, and photoelectronic effects of 3D mixed high-connected metal–organic frameworks based on octanuclear and dodecanuclear secondary building units. Dalton Trans 42(5):1567–1580
38. Wendlandt WW, Hecht HG (1966) Reflectance spectroscopy. Interscience, New York
39. Stylianou KC, Heck R, Chong SY, Bacsa J, Jones JT, Khimyak YZ, Bradshaw D, Rosseinsky MJ (2010) A guest-responsive fluorescent 3D microporous metal–organic framework derived from a long-lifetime pyrene core. J Am Chem Soc 132(12): 4119–4130
40. Zhang Y-N, Wang H, Liu J-Q, Wang Y-Y, Fu A-Y, Shi Q-Z (2009) Novel silver (I) compounds assembled from hybrid ligands based on linear or T-shaped coordination environment. Inorg Chem Commun 12(7):611–614
41. Hao J-M, Yu B-Y, Van Hecke K, Cui G-H (2015) A series of d^{10} metal coordination polymers based on a flexible bis (2-methylbenzimidazole) ligand and different carboxylates: synthesis, structures, photoluminescence and catalytic properties. CrystEngComm 17(11):2279–2293